LANGMUIR

pubs.acs.org/Langmuir Article

Linescan Lattice Microscopy: A Technique for the Accurate Measurement and Mapping of Lattice Spacing and Strain with Atomic Force Microscopy

J. Brandon McClimon, Zac Milne, Kathryn Hasz, and Robert W. Carpick*



Cite This: Langmuir 2021, 37, 8261-8269



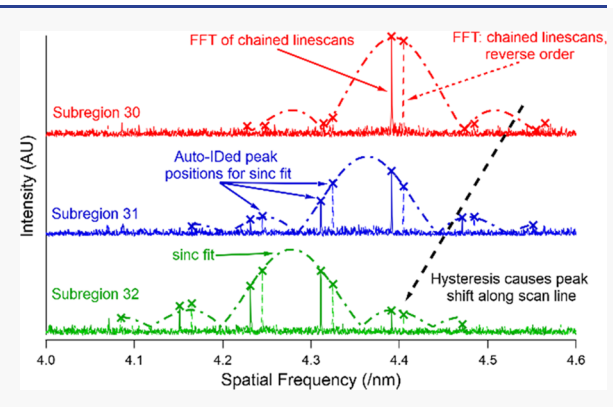
ACCESS

III Metrics & More

Article Recommendations

S Supporting Information

ABSTRACT: Lateral resolution and accuracy in scanning probe microscopies are limited by the nonideality of piezoelectric scanning elements due to phenomena including nonlinearity, hysteresis, and creep. By taking advantage of the well-established atomic-scale stick-slip phenomenon in contact-mode atomic force microscopy, we have developed a method for simultaneously indexing and measuring the spacing of surface atomic lattices using only Fourier analysis of unidirectional linescan data. The first step of the technique is to calibrate the X-piezo response using the stick-slip behavior itself. This permits lateral calibration to better than 1% error between 2.5 nm and 9 μ m, without the use of calibration gratings. Lattice indexing and lattice constant determination are demonstrated in this way on the NaCl(001) crystal surface. After piezo calibration, lattice constant measurement on



a natural bulk $MoS_2(0001)$ surface is demonstrated with better than 0.2% error. This is used to measure nonuniform thermal mismatch strain for chemical vapor deposition (CVD)-grown monolayer MoS_2 as small as 0.5%. A spatial mapping technique for the lattice spacing is developed and demonstrated, with absolute accuracy better than 0.2% and relative accuracy better than 0.1%, within a map of $12.5 \times 12.5 \text{ nm}^2$ pixels using bulk highly oriented pyrolytic graphite (HOPG) and MoS_2 as reference materials.

INTRODUCTION

The family of scanning probe microscopies (SPM), encompassing many modes of atomic force microscopy (AFM) as well as scanning tunneling microscopy (STM), are an important set of tools in modern research. As an area of scanning probe research, atomic resolution of surface crystal lattices has achieved broad success, for example, shedding light on details of the surface reconstruction of free surfaces which are relevant to catalysis and thin-film growth and properties. 1-3 Likewise, atomically resolved SPM is ideal for the study of local atomic defects, especially in thin-film systems.⁴⁻⁷ At the extreme end of such systems are two-dimensional (2D) materials like MoS₂ and graphene which have experienced explosive research interest in recent years. In such materials, atomic-scale structures like point defects, 8,9 nanobubbles/ wrinkles, 10,11 and stacking geometry in the case of few-layer films, 12,13 can have profound effects on local and global properties, and these structures and the resulting properties are often studied with scanning probe techniques.

Despite their enormous success, scanning probe methods have some inherent limitations. A significant one, particularly in the case of AFM, is lateral resolution, which stems from multiple sources. Lateral interactions with protrusions on the sample cause a convolution of the sample image with that of the AFM probe tip, which degrades the lateral resolution of

small sample features.¹⁴ Another source is from the scanning hardware. Most typically, the raster motion required is achieved with ceramic piezoelectric elements, often composed of a sintered lead zirconate (PZT) powder, which can be formulated to achieve a large piezoelectric coefficient, allowing for substantial piezoelectric displacement with practical bias voltages. The precision of such manipulators can be high, especially for small scan sizes, enabling the acquisition of atomically resolved images across spans of tens of nanometers or larger. Nevertheless, several inherent characteristics of these piezo ceramics limit lateral resolution. Such effects include increasing nonlinearity of response with increasing scan size and frequency due to piezo hysteresis and piezo creep. 15-17 Some commercial systems correct for these issues by implementing lateral position sensors and feedback control, which can correct the piezo position to below a few nanometers, but this can also degrade atomically resolved imaging due to additional noise caused by feedback systems.¹⁸

 Received:
 April 14, 2021

 Revised:
 June 6, 2021

 Published:
 June 25, 2021





Due to these limits of scanning probe lateral resolution, one aspect of the atomic structure has typically remained inaccessible without recourse to other techniques: the variation in bond lengths and the lattice constant due to, for example, temperature changes or lattice mismatch with a bulk substrate. Such lattice strain information can be determined at a local level if the sample is amenable to the preparation required for transmission electron microscopy or at a global level if the sample bulk is large enough to be probed using X-ray diffraction.¹⁹ Indirect techniques have also been developed, e.g., the Raman measurement of the lattice strain of MoS2 and graphene where benchmarking indicates substantial success. Lateral resolution is limited to the um scale due to the diffraction limit in conventional (far field) Raman microscopy. 20-22 Recently, a tip-enhanced Raman scheme has been developed. The method uses especially prepared silver nanowire-tipped probes with nanocubes of silver also mounted to the nanowire to improve the efficiency of the nanoantenna and therefore suppress background Raman excitation. This technique can achieve nanoscale strain mapping for materials where Raman spectral shifts can be correlated with strain states.²³ One additional scanning probe-based strain measurement technique with nanoscale resolution has been developed which maps relative strain via direct analysis of real-space images, but this technique has only been demonstrated at nearabsolute zero temperatures.²⁴ Strain information can be important since lattice strain can have a significant effect on overall material properties. The ability to measure local strains can prove useful, given that, e.g., in the case of graphene, nanostructuring can be combined with lattice strain to achieve useful modulation of electronic and optical properties.²⁵⁻

This study demonstrates a straightforward technique, which we will call linescan lattice microscopy (LLM), using an unmodified commercial AFM and unmodified commercial AFM tip/cantilever probes to measure the lattice constant and orientation for materials. The method works when the tip exhibits atomic-lattice stick-slip instabilities, which arise from the atomic surface corrugation in contact-mode AFM imaging and have been seen for a wide variety of materials.²⁸ The presence of such instabilities can be affected by the overall sharpness of the AFM probe or even the arrangement of atoms at the tip apex, which can cause the stick-slip instability to be extinguished along some or all scanning directions relative to the sample orientation.^{29,30} For materials that commonly exhibit the lattice stick-slip instability (i.e., ordered materials with uniform surfaces), switching to a new probe can often solve issues resolving the stick-slip instability. As well, recent results show that while polar anisotropy and left-right asymmetry can occur depending on the atomic structure of the tip, the overall periodicity can still remain the same, i.e., it still reflects the periodicity of the lattice.³⁰ Here, LLM is introduced and first used to provide a highly accurate scanner piezo calibration scheme valid across large length scales. The degree of absolute accuracy achieved is demonstrated by directly measuring the lattice constant of natural and CVDgrown monolayer MoS2 and by demonstrating that lattice strains in the CVD MoS₂ as small as 0.5% can be reliably measured.

■ RESULTS AND DISCUSSION

Figure 1a shows a fast Fourier transform (FFT) generated from a lattice-resolved contact-mode image of the (0001) surface of a bulk MoS_2 crystal. The corresponding real-space

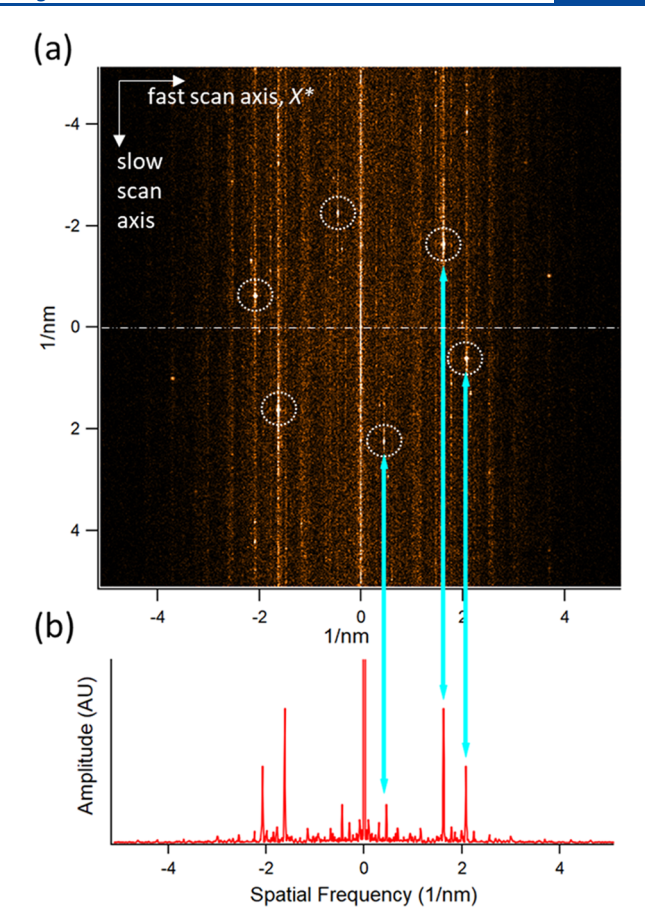


Figure 1. (a) Image FFT of the lateral force channel of a 2D lattice-resolved contact-mode AFM image of bulk MoS_2 using an AD-I-0.5-AS probe. The AFM scanning axes are identified and the diffraction spots are circled with dotted lines. The X^* -axis is the fast scanning axis in the real-space image. (b) Single linescan (dashed horizontal line in (a)) spanning the X^* -axis of the same image. The linescan shows that the intensity associated with all diffraction spots is present.

image is shown in Figure S1 of the Supporting Information (SI). Figure 1b shows a fast Fourier transform (FFT) generated from a single linescan in the same image, which illustrates the features enabling LLM. Three peaks are apparent in the spectrum (along with their expected reflections at negative spatial frequencies), which correspond to the Xcomponents of the three peaks in the associated image FFT. It is a common feature in image FFTs of atomic-lattice-resolved contact-mode images that intensity from diffraction spots extends along the slow scan axis, and it is this intensity that results in the peaks along the X-axis linescan regardless of which Y position is used. A mechanism involving slips from individual atomic positions can be used to explain these features. 28,31 The authors of ref 28 demonstrated that while scanning perpendicular to the cantilever axis, the tip apex can be pinned at atomic positions along multiple atomic rows in the cantilever axis position, leading to cantilever torsion that is detected as a variation in the lateral force signal. What was not appreciated about this phenomenon previously is that the slip behavior, even if stochastic at the level of individual slips, provides periodicity information about all close-packed atomiclattice directions perpendicular to the surface plane on a timeaveraged basis. Additionally, FFTs from atomic-lattice-resolved images, which contain diffraction spots extending along the slow scan direction, can also be found in the STM literature

where this slip mechanism is absent.^{32–35} The presence of these features in some STM work suggests that the following analysis could be amenable to other scanning probe techniques.

The ability to simultaneously measure the surface periodicity of all three close-packed planes on MoS_2 provides a means to measure the lattice constant and index the surface lattice of the sample with only an individual linescan. If it is assumed that the surface lattice is 6-fold symmetric, the reciprocal lattice constant can be calculated as

$$a^* = \frac{2\sqrt{X_1^{*2} + X_1^* X_2^* + X_2^{*2}}}{\sqrt{3}} \tag{1}$$

where X_1^* and X_2^* are the two lowest frequency peak spatial periodicities. Figure 2 illustrates relevant parameters and

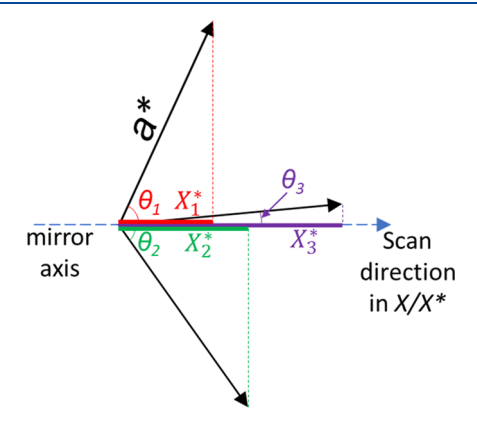


Figure 2. Schematic representation of the measured quantities in the 2D reciprocal space for a hexagonal lattice such as graphite or MoS₂. A mirror symmetry exists for the measurement across the scan direction axis.

geometry. Similar simple relations can be obtained for other possible peak pairs. If the lattice parameter is known, the reciprocal lattice orientation can be obtained from

$$\theta_i = \frac{X_i^*}{a^*} \tag{2}$$

For 6-fold symmetric axes, an ambiguity remains due to a mirror axis in the linescan direction. This can be resolved by inspection of the real-space normal force channel of the same linescan. As demonstrated in ref 28, the tip tends to slip along the close-packed plane of atoms oriented closest to the linescan direction, thereby sequentially increasing the buckling force on the cantilever (buckling and torsional cantilever deformations are illustrated in Figure S2c). When the tip slips between these close-packed rows, there is a reduction in the buckling force. With knowledge of the AFM coordinate system and the approximate frequency with which these slips occur, the direction of the change in normal force during slip unambiguously resolves whether the associated diffraction spot lies above or below the mirror axis. The lattice orientation determined in this fashion will be more accurate than one obtained from 2D imaging due to the lack of piezo creep along the slow scan direction and can be obtained with less tip wear since the acquisition of only a small number of linescans is required.

Now we consider an approach in which individual linescans were not analyzed, but rather time-resolved FFTs were captured by the AFM software from normal and lateral force channels. These were obtained from continuously scanning a single line with triangle-wave excitation of the scanner piezos, i.e., applying a triangle wave to the X-piezo with no Y-piezo actuation, to improve the signal-to-noise ratio and simplify the measurement. Because each analyzed force trace was long enough temporally to span many periods of the triangle excitation waveform, there are phase shifts in the stick-slip signal every time the probe tip reverses direction which affect the FFT of the force trace. These phase shifts cause the broad FFT peak near a single stick-slip frequency to be broken up into a comb structure. This is demonstrated in Figure 3 for the

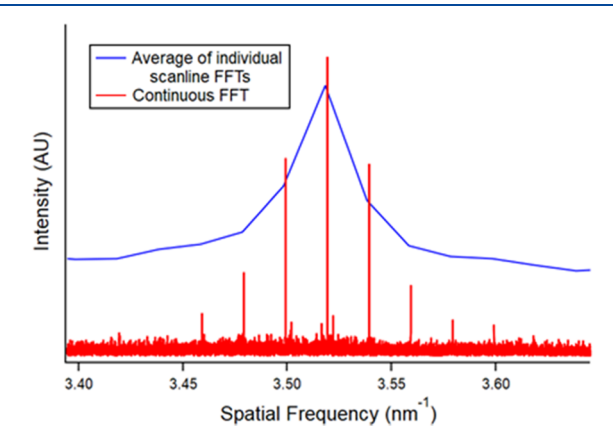


Figure 3. FFTs from a $50 \times 50 \text{ nm}^2$, $1024 \times 1024 \text{ pixel}^2$ image computed in two different ways: averaging FFTs from 1024 individual scan lines (blue data) or combining all data into a single one-dimensional (1D) line prior to FFT (red data). The data bracket a single atomic stick-slip peak. An AD-I-0.5-AS AFM probe was used.

case of spatially resolved data. The spacing of the spikes in the comb structure is equal to the inverse of the linescan length (or linescan duration for temporally resolved data). This spacing of the spikes in the comb structure is also equal to the spacing of the data points in the FFT of an individual linescan, so the useful frequency resolution remains unchanged. In both cases, longer linescan lengths not only correspond to the higher useful frequency resolution of the stick-slip periodicity, but also broadening of the peak or comb structure due to increasing piezo hysteresis.

Scanner Piezo Calibration. The measurement discussed above forms the basis for a new scanner piezo calibration technique that can, in principle, be valid across any length scale. Drift has minimal effect on the result since scanning speeds can be very high relative to any plausible drift rate, rendering the drift error negligible. In principle, drift errors can also be corrected in this technique, see the SI for details. By measuring the lattice constant in this fashion on a reference sample (natural MoS₂ in the following), accurate piezo calibration constants can be determined for the length scale of interest. For the data presented here, while scanning the sample surface in a reciprocating pattern at frequencies between 0.5 and 5 Hz, data was captured at a rate of 97.6 kHz, for 5.369 s, and an FFT performed. Twenty sequential FFTs were averaged to generate the spectrum for analysis, and the stick-slip frequencies chosen were those of maximum intensity.

A calibration curve from an RHK350 AFM is presented in Figure 4. The apparent lattice constant is plotted as a function of the maximum voltage of the triangle-wave piezo excitation

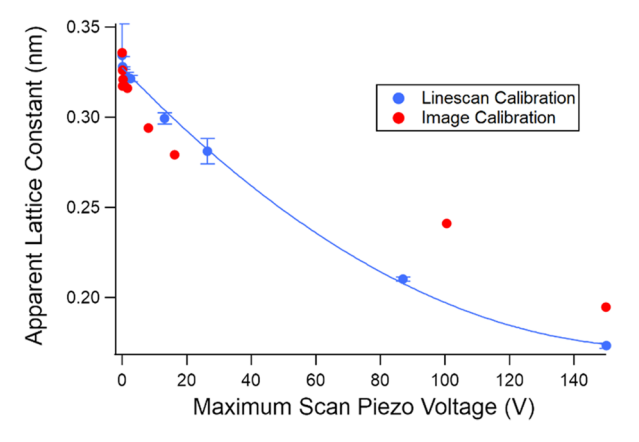


Figure 4. Calibration data for the AFM fast scan direction using an AD-I-0.5-AS AFM probe. Data are used to calculate the apparent lattice constant on a bulk $\rm MoS_2$ sample at a given maximum piezo voltage during the scan. The piezo calibration constant used was 30.785 nm/V. Red data points are from calibration using a 2D image FFT on bulk $\rm MoS_2$ for maximum scan piezo voltages <20 V (<500 nm) and using a TGZ1 calibration grating (NT-MDT, Moscow, Russia) for the scans longer than 3 μ m. Blue data points come from using the linescan FFT technique discussed in the manuscript, also on bulk $\rm MoS_2$. Error bars are the standard deviation of data obtained at a sequence of scan frequencies (listed in the SI) between 0.5 and 5 Hz. The solid line is a quadratic fit to the linescan calibration data.

(i.e., the lateral scan size). The data show the lattice constant which is calculated for different scan sizes assuming a constant piezo calibration value of 30.785 nm/V. This apparent lattice constant can be used to correct the piezo calibration value at each particular scan size to bring the apparent lattice constant into an agreement with the literature value of 0.3161 nm for MoS₂. The decreasing apparent lattice constant with increasing scan size could be well-fit by a quadratic trendline, 36 which allows for accurate calibration at any scan length between 2.5 nm and 9.2 µm. It can be seen from the error bars that the dependence on scanning frequency between 0.5 and 5 Hz is small. It can also be seen that an alternative calibration, performed with a combination of image FFTs at small image sizes and a calibration grating at large image sizes, provides a much less precise calibration. Part of the success of this calibration lies in the fact that there is no slow scan direction (i.e., image formation with the "Y" piezo) where creep, sample drift, and other effects limit the accuracy. In practice, of course, most experiments involve forming images where these effects will be present. Nevertheless, this calibration represents a large improvement over popular existing methods without an increase in experimental effort. One shortcoming of the technique in contact-mode AFM is that this calibration only applies to the X-piezo, so an equal sensitivity for the Y-piezo must be assumed. In the case that lattice resolution can be achieved while scanning parallel to the cantilever axis (stickslip contrast can be obtained in contact mode while scanning in this direction, ²⁸ see Figure S2a,b), the other piezo sensitivity may be calibrated independently with LLM.

In addition to hexagonal lattices such as MoS₂ and graphite, LLM was extended to cover the calculation of square lattices. Measurements identical to those described for the calibration above were performed on single-crystal NaCl(001) samples, for which atomic-lattice resolution was obtained. Only two stick-slip periodicities are available for calculation on this

surface, so the equation to calculate the reciprocal lattice constant takes the simpler form

$$a^* = \sqrt{X_1^{*2} + X_2^{*2}} \tag{3}$$

For a linescan size of 100 nm and a scan frequency of 1 Hz, using the calibration constant for that scan size determined from Figure 4, the lattice constant for NaCl was measured to be 0.3992 nm. It is typical for only one of the two ion types to be resolved in scanning probe studies.^{37,38} In such a case, the expected lattice constant is 0.3988 nm, in close agreement (0.10%) with the value we measured. Further details of this measurement are provided in the SI.

Measurement of Lattice Strain. To demonstrate the utility of the method in single-point lattice strain measurements, LLM was utilized to measure the in-plane strain at several specific points on CVD-grown monolayer MoS_2 on a SiO_2 substrate. Similar films have been shown to have an average tensile lattice strain of 0.4-1%, 22,39 due to the mismatch in thermal expansion coefficient between the SiO_2 and the MoS_2 and the fact that the samples are grown above $700~^{\circ}C$. Due to the symmetry assumptions of LLM, measured strain values assume that the strain is isotropic in the surface plane, which may not generally be the case. Nevertheless, Figure 5 shows the results of strain measurements at three

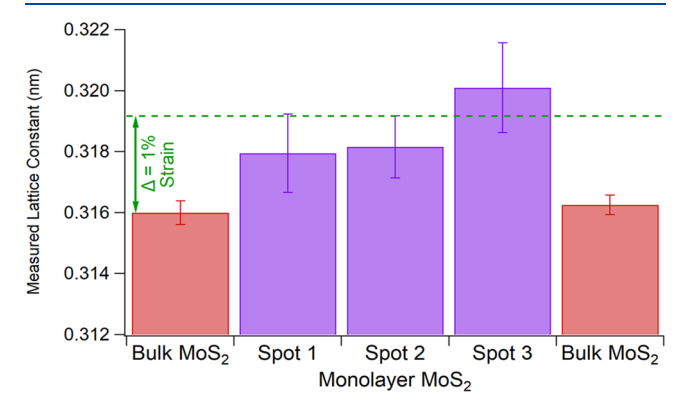


Figure 5. Lattice constants measured on bulk and CVD-grown monolayer MoS_2 with an AD-I-0.5-AS AFM probe. Data are captured by continuous scanning at 500 nm/s across a 50 nm scan length. Data are shown in the order in which they were obtained. After 20 min of scanning to stabilize the piezo trajectory, force data was obtained at 97.7 kHz for 5.369 s and an FFT was performed. Twenty sequential FFTs were averaged within the AFM software to create a spectrum for analysis. Error bars are the standard deviation of the lattice constant calculated from at least five spectra. The calibration constant of the microscope was adjusted to ensure that the first measurement on bulk MoS_2 was centered at the literature value 0.3161 nm.

specific locations on the CVD MoS_2 (images of the surrounding topography and friction force response are shown in the SI). The scan size, and hence the lateral resolution, of these measurements was 50 nm (as compared to 1 μ m for Raman⁴⁰ and 2 μ m for synchrotron-based X-ray diffraction⁴¹). Measurements on bulk MoS_2 were performed before and after the CVD MoS_2 measurements to confirm that the piezo behavior did not drift during the measurement. The average strain was found to be 0.83%. This value is within the range of previous measurements. ^{22,39,42}

2D Lattice Constant Mapping. To evaluate whether LLM can be extended to allow for 2D lattice constant mapping, a more sophisticated analysis was developed. To

validate the accuracy of the method, the measurement of the spatially resolved lattice constant was performed on an HOPG sample, for which the lattice constant at all locations is known a priori, allowing for the determination of absolute error. The method requires the acquisition of a high pixel-density 2D image that is subsequently subdivided to measure the lattice constant in individual subregions. Each subregion force image was redimensioned into a single 1D trace, creating data analogous to the time-resolved data acquisitions discussed above. For the demonstration below, the overall image was 100 \times 100 nm², 2048 \times 2048 pixel². As alluded to earlier, when the analyzed segment length is reduced, the spikes in the FFT comb structure separate. This unacceptably degrades the frequency resolution, and therefore the accuracy of the measured lattice constant, if the frequency of the most intense spike is used for the stick-slip frequency. To restore accuracy to the measurement, we chose to fit the envelope of the comb structure. By simulating a continuous sawtooth wave with periodic phase shifts (see the SI), it was determined that the appropriate fitting function for the FFT was

$$F(f) = y_{\text{off}} + A | \text{sinc} \left(T[f - f_0] \right) | \tag{4}$$

where F(f) is the spectral intensity, $y_{\rm off}$ is a y-offset to account for the background intensity, A is the amplitude of the envelope, T is the inverse of the segment length, which is known, and f_0 is the stick-slip frequency of interest. An identical functional form can be found in the pulsed wave radar literature, where a rectangular pulse train signal bears some similarities to the stick-slip signal here.

To accomplish the fitting, a program was written in IgorPro (v7, Wavemetrics, Portland, OR) that automatically extracts the position and amplitude of each of the FFT spikes across a specified range corresponding to each of the stick-slip frequencies and fits them with the sinc equation given above. This program also generated additional data points to improve the fit by analyzing the same subregion, but with the order in which the scan lines are stitched together reversed. Because this changes the phase shift between subsequent scan lines, the positions of the FFT spikes change. The IgorPro program is included in the SI. An example of the fitting results is shown in Figure 6a for an image of HOPG. The stick-slip frequency shifts between subsequent subregions are due to piezo hysteresis.

To convert the measurement into an accurate lattice constant measurement, given the hysteresis in the piezo trajectory, identical reference measurements on a bulk MoS₂ sample were performed before and after the HOPG measurement. Since the lattice constant of the bulk MoS2 is known, the apparent lattice constant measured on the MoS2 for each of the subregions could be used to correct the HOPG lattice constants for piezo hysteresis. When this was done, the map shown in Figure 6b could be generated, with a color scale spanning 1% of the true lattice constant. From the map data shown in Figure 6c, it is clear that the relative error between subregions within the map was very small. The standard deviation was 0.06%. To determine the absolute error that could be expected from a lattice constant measurement such as this, the entire procedure was repeated four times at four different locations on the HOPG and eight different locations on the MoS₂ for the reference measurements. The standard deviation of the absolute error (deviation from the HOPG literature value of 0.2461 nm) for these measurements was 0.19%. This also demonstrates the insensitivity of the

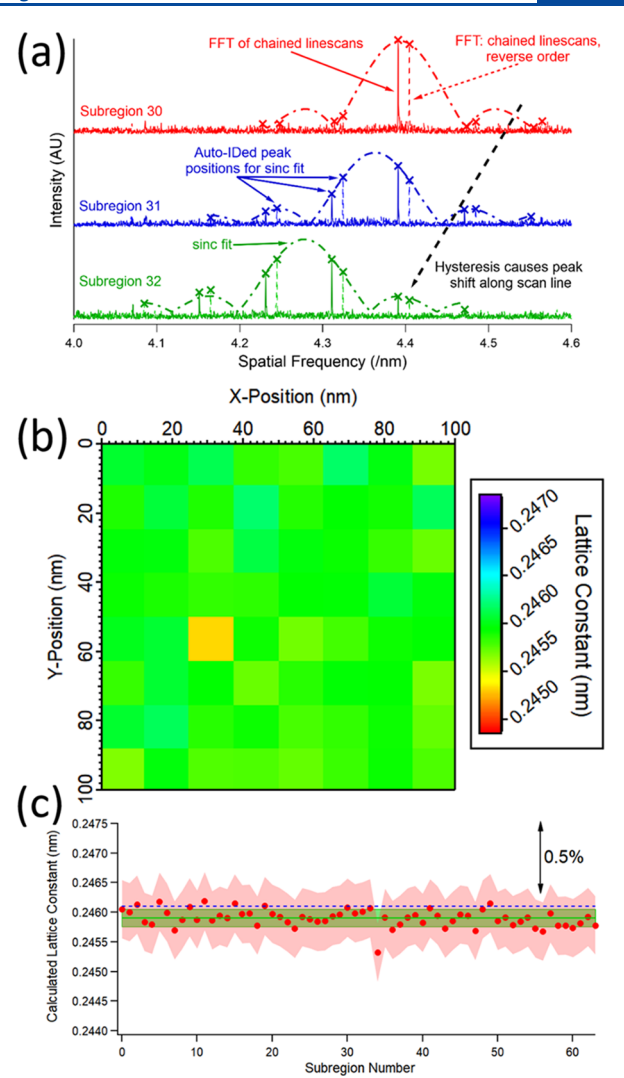


Figure 6. (a) Example fitting of the lateral force FFT to determine the stick-slip frequency for three sequential subregions of a 100×100 nm² image of HOPG using an ND-CTI AFM probe, which has been subdivided into 8×8 equal regions. (b) Map of the lattice constants determined for the HOPG image in (a). Each subregion is 12.5 nm square. (c) Same data as in (b). The green envelope is the standard deviation of the data. The red envelope is the absolute error of the measurement determined by repeating the measurement four times. The dotted line is at the true lattice constant for HOPG. The 0.5% scale illustrates the typical units for lattice strain.

measurement to relative sample orientation. Given the small typical grain size of the grade ZYH HOPG, <1 μ m, each of the four measurements was almost certainly performed on a fresh grain with a random orientation, yet in all cases, the average calculated lattice constant was close to the literature value within a very small standard deviation.

Sine Wave Excitations. While most AFM work is done using triangle-wave piezo excitation to allow for image formation, there are techniques such as lateral stiffness measurement and circle scanning 47,48 which require knowledge of the absolute lateral displacement amplitude of a high-frequency sine wave piezo excitation. Accurate knowledge of this parameter is difficult to achieve, given the dependence of piezo trajectories on scanning frequency and excitation amplitude. To address this calibration difficulty, LLM was extended to the case of sine piezo oscillations.

Measurements were performed identically to the time-resolved measurements discussed above, except with a sine wave oscillation. Since the tip speed is not constant during the sine oscillation, the FFT does not show discrete peaks corresponding to the stick-slip frequency; however, near the maximum speed of the waveform, the speed does not change rapidly, which provides a recognizable peak in the FFT. If the stick-slip frequency at the maximum speed during the oscillation can be ascertained from the FFT, calculating the amplitude of the piezo oscillation is straightforward (see the SI)

$$amplitude = \frac{f_{FFT}}{2\pi f_{osc} \xi_{latt}}$$
 (5)

where $f_{\rm FFT}$ is the stick-slip frequency obtained from the FFT, $f_{\rm osc}$ is the oscillation frequency of the piezo excitation, and $\xi_{\rm latt}$ is the spatial frequency of the lattice in the scanning direction. $\xi_{\rm latt}$ must be determined from an image FFT or standard LLM with a triangle-wave excitation.

Simulations of the force signal expected for a sinusoidal oscillation above a periodic surface lattice were performed, and the results Fourier transformed, shown in Figure 7a. The blue line represents the true frequency of the stick-slip at the maximum tip speed during oscillation. The slight underestimate (0.5-3.5% for amplitudes of 2-20 nm) of the true stick-slip frequency will lead to a similar underestimate of the oscillation amplitude. This error could be corrected by performing simulations similar to Figure 7a for the experimental parameters to determine a correction factor for the experimental data. Figure 7b shows an FFT of an experimental force trace during a sinusoidal oscillation of 23 nm amplitude and 50 Hz on natural MoS₂. Aside from the presence of multiple peaks $(f_2 \text{ and } f_3)$ due to slips across each of the close-packed directions, the FFT is qualitatively similar to the simulated result. Figure 7c shows calibration curves calculated using the above equation for oscillations at multiple amplitudes and 5, 50, and 500 Hz. Over this frequency range, the variation of the true oscillation amplitude is small. The variation is a consequence of hysteresis in piezoelectric actuators.⁴⁹ By projecting linear fits back to zero excitation, the amplitudes of sub-nm excitations can be accurately calibrated, which is required for some oscillation techniques, such as the lateral stiffness measurement.4

CONCLUSIONS

The set of techniques developed here present useful calibration methods for open-loop scanning probe microscopes. In particular, the ability to calibrate various length scales equally well without substantial additional effort is particularly useful. Multiple calibration gratings are typically used for this purpose, and the limited variety of commercial gratings, particularly for the sub- μ m length scale, creates difficulty. Calibration by taking FFTs of atomically resolved crystal lattice images can only be performed on the tens of nm length scale before the calibration becomes extremely time-consuming and data-intensive, as well as increasing the likelihood of tip wear.

The lattice constant mapping technique discussed above could prove useful for mapping strain on atomically resolved lattices presuming that the lattice strains are predominantly isotropic. In cases where strains are substantially nonisotropic, the symmetry assumptions of LLM break down. For the spot mapping of lattice strain on monolayer CVD MoS₂, we attribute our success to the fact that the tensile strain is

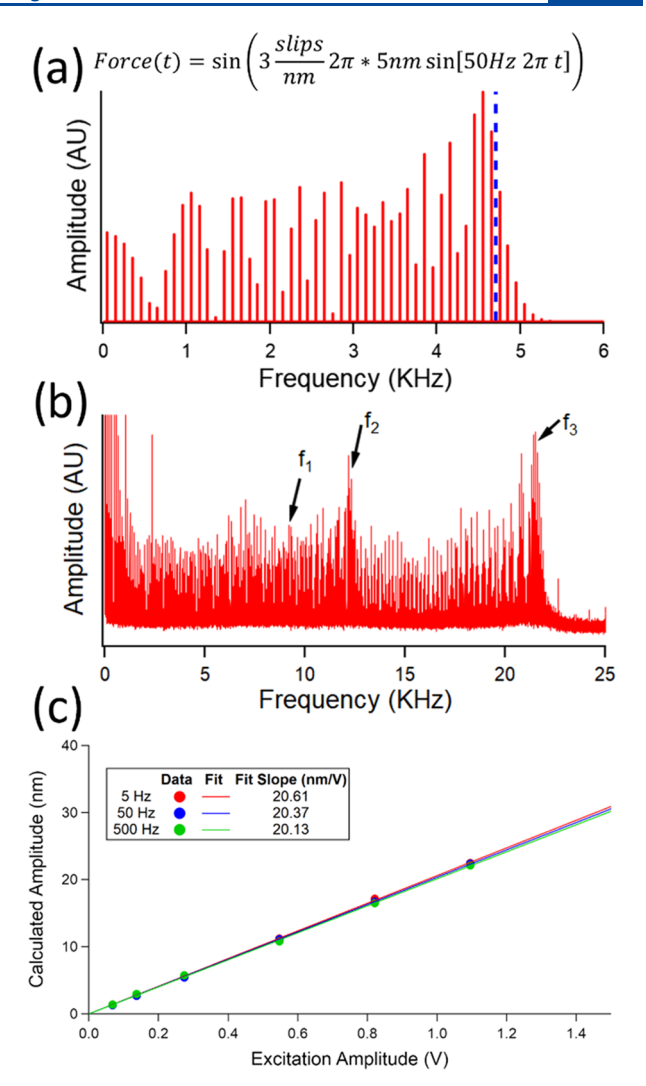


Figure 7. (a) FFT of simulated force trace generated from the listed equation which simulates a 5 nm, 50 Hz sin oscillation on a material with a lattice periodicity of 3 nm $^{-1}$. (b) Experimental FFT of lateral force trace on natural MoS $_2$ using an HQ:CSC37/Al AFM probe while oscillating tip at 50 Hz with an amplitude calculated to be 23 nm. f_1 is identified on the basis of lattice symmetry. (c) Calibration curves for the sine oscillation technique at 50 and 500 Hz.

expected to be reasonably isotropic and that the measurement sampled a 50 nm long region which averaged out local strain orientations. A natural extension of LLM to strengthen the strain mapping capability would be to perform scans in two perpendicular directions over the same region sequentially. This would allow for the construction of high-resolution 2D FFTs for arbitrary crystalline lattices and thereby unambiguously measure arbitrary local strain states. Scanning along the axis of the cantilever beam is problematic in contact-mode AFM due to the convolution of normal and buckling forces in the normal force signal channel and satisfactory measurements could not be achieved. No such limitation exists for noncontact scanning probe techniques, however. Another strategy to improve the technique would be to reduce the nonlinearity of the piezo response. While we have outlined a workable strategy to compensate for hysteresis, the signal-to-noise ratio of the force signal is improved as piezo linearity, and therefore the periodicity of the force signal, also improves. It is in fact possible to essentially eliminate hysteresis by exciting the piezo

with a controlled quantity of electric charge rather than controlling the excitation voltage. 50,51

The feasibility of LLM, in general, relies on the precision and long-time stability of the piezoelectric behavior of the AFM scanner. In fact, the AFM utilized here has certain features that make applying the technique more challenging. Specifically, coarse positioning, retract, and approach operations are all implemented via an inertial drive system, which requires scanner piezos to instantaneously cross their full range of motion repeatedly at high frequency. Nevertheless, after 20 min of stabilization time before making measurements, piezo trajectories were repeatable enough that high absolute accuracy could be demonstrated for a variety of lattice constant measurements. This implies that other microscope designs could demonstrate even better performance, especially if piezos can be dedicated to making these measurements alone and are decoupled from other positioning operations.

This study demonstrates that individual linescans possess all of the information necessary to index and measure the lattice constant of crystalline surface lattices with a degree of accuracy unprecedented in the scanning probe literature. This allows for the fast (<2 min of data acquisition for each scan size) calibration of piezo lateral displacements at arbitrary length scales with high accuracy and no need for additional instrumentation or specialized samples aside from widely available reference samples such as HOPG, NaCl, or natural MoS₂. LLM was also demonstrated on the square lattice of NaCl. LLM also allows for the accurate measurement of lattice strain with a high lateral resolution, as was demonstrated in the case of monolayer CVD MoS₂. 2D mapping of the lattice constant with absolute accuracy as high 0.2% was also demonstrated on an HOPG reference sample. Finally, a calibration technique for determining the displacement of small sinusoidal oscillation down to the sub-nm length scale is demonstrated, which can be useful to improve the accuracy of oscillation-based measurements. In total, this provides the ability to conveniently and accurately calibrate the lateral motion of SPM systems, and to also map surface lattice strains of samples, including but not limited to 2D materials, with high accuracy and precision.

EXPERIMENTAL SECTION

All experiments discussed were performed in an RHK350 atomic force microscope with an R9 controller (RHK Tech., Troy, MI). The AFM was mounted in a vibration isolated environmental control chamber. Flowing N2 from the boiloff of a liquid nitrogen dewar was used to maintain <5% RH throughout the measurements. The AFM was operated in contact mode using primarily diamond-coated AFM probes (AD-I-0.5-AS, nominal normal spring constant (k_{norm}) of 0.5 N/m, Adama Innovations, Dublin, Ireland; ND-CTI series, k_{norm} = 0.46 N/m, Advanced Diamond Technologies, Romeoville, IL) for maximum wear resistance, though the technique was demonstrated with bare Si probes (HQ:CSC37/Al BS, $k_{\text{norm}} = 0.3 \text{ N/m}$, NanoAndMore, Watsonville, CA) as well. The probe type used is annotated in each figure caption. Contact-mode probes with normal spring constants below 1 N/m provide the most reliable results because a low torsional spring constant, which scales with the normal spring constant, is necessary to ensure the existence of the mechanical instability that leads to stick-slip tip motion.⁵³ Sample materials discussed include natural MoS2, NaCl single crystal, grade ZYH HOPG (Structure Probe Inc., West Chester, PA), and CVD-grown MoS₂ on a SiO₂ substrate. Measurements were performed via reciprocating scanning at various sizes and frequencies at low loads (<5 nN) while simultaneously capturing the normal and lateral force traces at sampling rates high enough that atomic-scale periodicities

could be extracted from Fourier transforms of this data (i.e., atomic-scale spatial frequencies were below the Nyqvist frequency of the sampling rate). Adhesion forces of 2–10 nN ensured that the tip stayed in contact at loads near 0 nN. Near-zero applied loads typically provided the strongest stick-slip signal. Also, low loads minimize the occurrence of double and triple slips which reduce the intensity of the FFT peaks of interest, ^{54,55} and, presumably, elastic distortions of the sample lattice at high loads might negatively affect the accuracy of LLM as well

ASSOCIATED CONTENT

Supporting Information

The Supporting Information is available free of charge at https://pubs.acs.org/doi/10.1021/acs.langmuir.1c01019.

Interpretation of FFTs, provenance of LLM equations, resolving lattice orientation ambiguity, scan parameters used in scanner piezo calibration, LLM on NaCl single crystal, drift correction in LLM, stick-slip simulations, CVD MoS₂ strain measurement, codes for 2D lattice constant mapping analysis, and sine wave oscillation (PDF)

AUTHOR INFORMATION

Corresponding Author

Robert W. Carpick — Department of Mechanical Engineering and Applied Mechanics, University of Pennsylvania, Philadelphia, Pennsylvania 19104, United States; orcid.org/0000-0002-3235-3156; Email: carpick@seas.upenn.edu

Authors

J. Brandon McClimon – Department of Materials Science and Engineering, University of Pennsylvania, Philadelphia, Pennsylvania 19104, United States; orcid.org/0000-0002-2163-7495

Zac Milne — Department of Mechanical Engineering and Applied Mechanics, University of Pennsylvania, Philadelphia, Pennsylvania 19104, United States; Present Address: Sandia National Laboratories, Albuquerque, New Mexico 87123, United States.; orcid.org/0000-0003-2000-5901

Kathryn Hasz — Department of Materials Science and Engineering, University of Pennsylvania, Philadelphia, Pennsylvania 19104, United States; Present Address: University of Colorado, Boulder, Colorado 80309, United States.

Complete contact information is available at: https://pubs.acs.org/10.1021/acs.langmuir.1c01019

Author Contributions

J.B.M. designed and conducted all experiments and analyzed experimental results. Z.M. and K.H. contributed to the experimental design and analysis of results. R.W.C. supervised all experimental work and analysis.

Notes

The authors declare no competing financial interest.

ACKNOWLEDGMENTS

This work was funded by the National Science Foundation, awards CMMI-1761874 and DMR-1720530 (the University of Pennsylvania MRSEC), and by the Air Force Office of Scientific Research under grant FA2386-18-1-4083.

■ REFERENCES

- (1) Song, Z.; Hrbek, J.; Osgood, R. Formation of TiO₂ Nanoparticles by Reactive-Layer-Assisted Deposition and Characterization by XPS and STM. *Nano Lett.* **2005**, *5*, 1327–1332.
- (2) Raiteri, P.; Migas, D. B.; Miglio, L.; Rastelli, A.; von Känel, H. Critical Role of the Surface Reconstruction in the Thermodynamic Stability of {105} Ge Pyramids on Si(001). *Phys. Rev. Lett.* **2002**, *88*, No. 256103.
- (3) Giessibl, F. J. Atomic Resolution of the Silicon (111)- (7×7) Surface by Atomic Force Microscopy. *Science* **1995**, 267, 68–71.
- (4) Ashworth, T. V.; Thornton, G. Thin Film TiO₂ on Nickel(110): An STM Study. *Thin Solid Films* **2001**, 400, 43–45.
- (5) Huijbregtse, J. M.; Dam, B.; van der Geest, R. C. F.; Klaassen, F. C.; Elberse, R.; Rector, J. H.; Griessen, R. Natural Strong Pinning Sites in Laser-Ablated YBa₂Cu₃O_{7-x} Thin Films. *Phys. Rev. B* **2000**, *62*, 1338–1349.
- (6) Hansen, P. J.; Strausser, Y. E.; Erickson, A. N.; Tarsa, E. J.; Kozodoy, P.; Brazel, E. G.; Ibbetson, J. P.; Mishra, U.; Narayanamurti, V.; DenBaars, S. P.; Speck, J. S. Scanning Capacitance Microscopy Imaging of Threading Dislocations in GaN Films Grown on (0001) Sapphire by Metalorganic Chemical Vapor Deposition. *Appl. Phys. Lett.* 1998, 72, 2247–2249.
- (7) Setvín, M.; Wagner, M.; Schmid, M.; S Parkinson, G.; Diebold, U. Surface Point Defects on Bulk Oxides: Atomically-Resolved Scanning Probe Microscopy. *Chem. Soc. Rev.* **2017**, *46*, 1772–1784.
- (8) Ziatdinov, M.; Fujii, S.; Kiguchi, M.; Enoki, T.; Jesse, S.; Kalinin, S. V. Data Mining Graphene: Correlative Analysis of Structure and Electronic Degrees of Freedom in Graphenic Monolayers with Defects. *Nanotechnology* **2016**, *27*, No. 495703.
- (9) Tumino, F.; Casari, C. S.; Li Bassi, A.; Tosoni, S. Nature of Point Defects in Single-Layer MoS2 Supported on Au(111). *J. Phys. Chem.* C 2020, 124, 12424–12431.
- (10) Levy, N.; Burke, S. A.; Meaker, K. L.; Panlasigui, M.; Zettl, A.; Guinea, F.; Neto, A. H. C.; Crommie, M. F. Strain-Induced Pseudo—Magnetic Fields Greater Than 300 Tesla in Graphene Nanobubbles. *Science* **2010**, 329, 544—547.
- (11) Xu, K.; Cao, P.; Heath, J. R. Scanning Tunneling Microscopy Characterization of the Electrical Properties of Wrinkles in Exfoliated Graphene Monolayers. *Nano Lett.* **2009**, *9*, 4446–4451.
- (12) Yankowitz, M.; Chen, S.; Polshyn, H.; Zhang, Y.; Watanabe, K.; Taniguchi, T.; Graf, D.; Young, A. F.; Dean, C. R. Tuning Superconductivity in Twisted Bilayer Graphene. *Science* **2019**, *363*, 1059–1064.
- (13) Zou, Z.; Carnevali, V.; Jugovac, M.; Patera, L. L.; Sala, A.; Panighel, M.; Cepek, C.; Soldano, G.; Mariscal, M. M.; Peressi, M.; Comelli, G.; Africh, C. Graphene on Nickel (100) Micrograins: Modulating the Interface Interaction by Extended Moiré Superstructures. *Carbon* **2018**, *130*, 441–447.
- (14) Villarrubia, J. S. Algorithms for Scanned Probe Microscope Image Simulation, Surface Reconstruction, and Tip Estimation. *J. Res. Natl. Inst. Stand. Technol.* **1997**, *102*, No. 425.
- (15) Bhikkaji, B.; Ratnam, M.; Fleming, A. J.; Moheimani, S. O. R. High-Performance Control of Piezoelectric Tube Scanners. *IEEE Trans. Control Syst. Technol.* **2007**, *15*, 853–866.
- (16) Jung, H.; Gweon, D.-G. Creep Characteristics of Piezoelectric Actuators. Rev. Sci. Instrum. 2000, 71, 1896–1900.
- (17) Hues, S. M.; Draper, C. F.; Lee, K. P.; Colton, R. J. Effect of PZT and PMN Actuator Hysteresis and Creep on Nanoindentation Measurements Using Force Microscopy. *Rev. Sci. Instrum.* **1994**, *65*, 1561–1565.
- (18) Fleming, A. J.; Leang, K. K. Charge Drives for Scanning Probe Microscope Positioning Stages. *Ultramicroscopy* **2008**, *108*, 1551–1557.
- (19) Cooper, D.; Denneulin, T.; Bernier, N.; Béché, A.; Rouvière, J.-L. Strain Mapping of Semiconductor Specimens with Nm-Scale Resolution in a Transmission Electron Microscope. *Micron* **2016**, *80*, 145–165.
- (20) He, R.; Zhao, L.; Petrone, N.; Kim, K. S.; Roth, M.; Hone, J.; Kim, P.; Pasupathy, A.; Pinczuk, A. Large Physisorption Strain in

- Chemical Vapor Deposition of Graphene on Copper Substrates. *Nano Lett.* **2012**, *12*, 2408–2413.
- (21) Ni, Z. H.; Yu, T.; Lu, Y. H.; Wang, Y. Y.; Feng, Y. P.; Shen, Z. X. Uniaxial Strain on Graphene: Raman Spectroscopy Study and Band-Gap Opening. *ACS Nano* **2008**, *2*, 2301–2305.
- (22) Chae, W. H.; Cain, J. D.; Hanson, E. D.; Murthy, A. A.; Dravid, V. P. Substrate-Induced Strain and Charge Doping in CVD-Grown Monolayer MoS₂. *Appl. Phys. Lett.* **2017**, *111*, No. 143106.
- (23) Ma, X.; Zhu, Y.; Yu, N.; Kim, S.; Liu, Q.; Apontti, L.; Xu, D.; Yan, R.; Liu, M. Toward High-Contrast Atomic Force Microscopy-Tip-Enhanced Raman Spectroscopy Imaging: Nanoantenna-Mediated Remote-Excitation on Sharp-Tip Silver Nanowire Probes. *Nano Lett.* **2019**, *19*, 100–107.
- (24) Zeljkovic, I.; Walkup, D.; Assaf, B. A.; Scipioni, K. L.; Sankar, R.; Chou, F.; Madhavan, V. Strain Engineering Dirac Surface States in Heteroepitaxial Topological Crystalline Insulator Thin Films. *Nat. Nanotechnol.* **2015**, *10*, 849–853.
- (25) Wang, Y.; Yang, R.; Shi, Z.; Zhang, L.; Shi, D.; Wang, E.; Zhang, G. Super-Elastic Graphene Ripples for Flexible Strain Sensors. *ACS Nano* **2011**, *5*, 3645–3650.
- (26) Zhong-Jun, L.; Qiang, L.; Zeng-Guang, C.; Hong-Bian, L.; Ying, F. Controlled Construction of Nanostructures in Graphene. *Chin. Phys. B* **2014**, 23, No. 028102.
- (27) Trung, T. Q.; Tien, N. T.; Kim, D.; Jang, M.; Yoon, O. J.; Lee, N.-E. A Flexible Reduced Graphene Oxide Field-Effect Transistor for Ultrasensitive Strain Sensing. *Adv. Funct. Mater.* **2014**, *24*, 117–124.
- (28) Morita, S.; Fujisawa, S.; Sugawara, Y. Spatially Quantized Friction with a Lattice Periodicity. Surf. Sci. Rep. 1996, 23, 1-41.
- (29) Tang, H.; Joachim, C.; Devillers, J. Interpretation of AFM Images: The Graphite Surface with a Diamond Tip. Surf. Sci. 1993, 291, 439–450.
- (30) Vazirisereshk, M. R.; Hasz, K.; Carpick, R. W.; Martini, A. Friction Anisotropy of MoS₂: Effect of Tip–Sample Contact Quality. *J. Phys. Chem. Lett.* **2020**, *11*, 6900–6906.
- (31) Mate, C. M.; McClelland, G. M.; Erlandsson, R.; Chiang, S. Atomic-Scale Friction of a Tungsten Tip on a Graphite Surface. *Phys. Rev. Lett.* **1987**, *59*, 1942–1945.
- (32) Aketagawa, M.; Takada, K. Correction of Distorted STM Image by Using a Regular Crystalline Lattice and 2D FFT. *Nanotechnology* **1995**, *6*, No. 105.
- (33) Feng, J.; Wagner, S. R.; Zhang, P. Interfacial Coupling and Electronic Structure of Two-Dimensional Silicon Grown on the Ag(111) Surface at High Temperature. *Sci. Rep.* **2015**, *5*, No. 10310.
- (34) Huang, B. M.; Lister, T. E.; Stickney, J. L. Se Adlattices Formed on Au(100), Studies by LEED, AES, STM and Electrochemistry. *Surf. Sci.* **1997**, 392, 27–43.
- (35) Joucken, F.; Frising, F.; Sporken, R. Fourier Transform Analysis of STM Images of Multilayer Graphene Moiré Patterns. *Carbon* **2015**, 83, 48–52.
- (36) Ai, C.; Wyant, J. C. Effect of Piezoelectric Transducer Nonlinearity on Phase Shift Interferometry. *Appl. Opt.* **1987**, *26*, 1112–1116
- (37) Glöckler, K.; Sokolowski, M.; Soukopp, A.; Umbach, E. Initial Growth of Insulating Overlayers of NaCl on Ge(100) Observed by Scanning Tunneling Microscopy with Atomic Resolution. *Phys. Rev. B* **1996**, *54*, 7705–7708.
- (38) Meyer, G.; Amer, N. M. Optical-beam-deflection Atomic Force Microscopy: The NaCl (001) Surface. *Appl. Phys. Lett.* **1990**, *56*, 2100–2101.
- (39) Liu, Z.; Amani, M.; Najmaei, S.; Xu, Q.; Zou, X.; Zhou, W.; Yu, T.; Qiu, C.; Birdwell, A. G.; Crowne, F. J.; Vajtai, R.; Yakobson, B. I.; Xia, Z.; Dubey, M.; Ajayan, P. M.; Lou, J. Strain and Structure Heterogeneity in MoS₂ Atomic Layers Grown by Chemical Vapour Deposition. *Nat. Commun.* **2014**, *5*, No. 5246.
- (40) Fu, Y.; Ding, X.; Li, J.; Zhang, J. A Novel Knife-Edge Method for Measuring the Lateral Resolution of Confocal Raman Microscopes. In *AOPC 2019: Optical Spectroscopy and Imaging*; International Society for Optics and Photonics, 2019; Vol. 11337, p113370B.

- (41) Ristanović, Z.; Hofmann, J. P.; Deka, U.; Schülli, T. U.; Rohnke, M.; Beale, A. M.; Weckhuysen, B. M. Intergrowth Structure and Aluminium Zoning of a Zeolite ZSM-5 Crystal as Resolved by Synchrotron-Based Micro X-Ray Diffraction Imaging. *Angew. Chem.* **2013**, *125*, 13624–13628.
- (42) Luo, S.; Cullen, C. P.; Guo, G.; Zhong, J.; Duesberg, G. S. Investigation of Growth-Induced Strain in Monolayer MoS₂ Grown by Chemical Vapor Deposition. *Appl. Surf. Sci.* **2020**, *508*, No. 145126.
- (43) Brandwood, D. Fourier Transforms in Radar and Signal Processing, 2nd ed.; Artech House, 2012; p 63.
- (44) Carpick, R. W.; Ogletree, D. F.; Salmeron, M. Lateral Stiffness: A New Nanomechanical Measurement for the Determination of Shear Strengths with Friction Force Microscopy. *Appl. Phys. Lett.* **1997**, *70*, 1548–1550.
- (45) Piétrement, O.; Beaudoin, J. L.; Troyon, M. A New Calibration Method of the Lateral Contact Stiffness and Lateral Force Using Modulated Lateral Force Microscopy. *Tribol. Lett.* **1999**, *7*, 213–220.
- (46) McClimon, J. B.; Hilbert, J.; Lukes, J. R.; Carpick, R. W. Nanoscale Run-In of Silicon Oxide-Doped Hydrogenated Amorphous Carbon: Dependence of Interfacial Shear Strength on Sliding Length and Humidity. *Tribol. Lett.* **2020**, *68*, No. 80.
- (47) Yong, Y. K.; Moheimani, S. O. R.; Petersen, I. R. High-Speed Cycloid-Scan Atomic Force Microscopy. *Nanotechnology* **2010**, *21*, No. 365503.
- (48) Nasrallah, H.; Mazeran, P.-E.; Noël, O. Circular Mode: A New Scanning Probe Microscopy Method for Investigating Surface Properties at Constant and Continuous Scanning Velocities. *Rev. Sci. Instrum.* **2011**, *82*, No. 113703.
- (49) Zhu, W.; Rui, X.-T. Hysteresis Modeling and Displacement Control of Piezoelectric Actuators with the Frequency-Dependent Behavior Using a Generalized Bouc–Wen Model. *Precis. Eng.* **2016**, 43, 299–307.
- (50) Newcomb, C. V.; Flinn, I. Improving the Linearity of Piezoelectric Ceramic Actuators. *Electron. Lett.* **1982**, *18*, 442–444.
- (51) Minase, J.; Lu, T.-F.; Cazzolato, B.; Grainger, S. A Review, Supported by Experimental Results, of Voltage, Charge and Capacitor Insertion Method for Driving Piezoelectric Actuators. *Precis. Eng.* **2010**, *34*, 692–700.
- (52) Brukman, M. J.; Carpick, R. W. Vibrations of the "Beetle" Scanning Probe Microscope: Identification of a New Mode, Generalized Analysis, and Characterization Methodology. *Rev. Sci. Instrum.* 2006, 77, No. 033706.
- (53) Li, Q.; Dong, Y.; Perez, D.; Martini, A.; Carpick, R. W. Speed Dependence of Atomic Stick-Slip Friction in Optimally Matched Experiments and Molecular Dynamics Simulations. *Phys. Rev. Lett.* **2011**, *106*, No. 126101.
- (54) Medyanik, S. N.; Liu, W. K.; Sung, I.-H.; Carpick, R. W. Predictions and Observations of Multiple Slip Modes in Atomic-Scale Friction. *Phys. Rev. Lett.* **2006**, *97*, No. 136106.
- (55) Roth, R.; Glatzel, T.; Steiner, P.; Gnecco, E.; Baratoff, A.; Meyer, E. Multiple Slips in Atomic-Scale Friction: An Indicator for the Lateral Contact Damping. *Tribol. Lett.* **2010**, *39*, 63–69.